GALACTIC FOREGROUND CONSTRAINTS FROM THE PYTHON V COSMIC MICROWAVE BACKGROUND ANISOTROPY DATA

Pia Mukherjee,[1,2] Kim Coble,[3,4] Mark Dragovan,[5] Ken Ganga,[6] John Kovac,[3]
Bharat Ratra,[1] and Tarun Souradeep[1,7]

ABSTRACT

We constrain Galactic foreground contamination of the Python V cosmic microwave background anisotropy data by cross-correlating it with foreground contaminant emission templates. To model foreground emission, we use 100 and 12 μm dust templates and two point-source templates based on the Parkes-MIT-NRAO survey. The analysis takes account of intermodulation correlations in eight modulations of the data that are sensitive to a large range of angular scales and also densely sample a large area of sky. As a consequence, the analysis here is highly constraining. We find little evidence for foreground contamination in an analysis of the whole data set. However, there is indication that foregrounds are present in the data from the larger angular scale modulations of those Python V fields that overlap the region scanned earlier by the University of California at Santa Barbara South Pole 1994 experiment. This is an independent consistency cross-check of findings from the South Pole 1994 data.

Subject headings: cosmic microwave background — cosmology: observations — diffuse radiation — dust, extinction

1. INTRODUCTION

While cosmic microwave background (CMB) anisotropy data have started to provide interesting constraints on cosmological parameters (see, e.g., Podariu et al. 2001; Page 2002; Mukherjee et al. 2003a, 2003b; Benoît et al. 2003; Ruhl et al. 2002; Kuo et al. 2002; Slosar et al. 2002 for recent results; Peebles & Ratra 2003 for a review), Galactic emission foreground contaminants in them are still not well understood. Robust constraints on cosmological parameters from these data require a better understanding of the effect of these contaminants.

In this paper we study foreground contaminants in the Python V (PyV) CMB anisotropy data. PyV is the latest of the Python experiments at the South Pole. Coble et al. (1999, 2003) describe the PyV experiment, observations, and data reduction. Dragovan et al. (1994), Ruhl et al. (1995), and Platt et al. (1997) describe Python I–III, and Rocha et al. (1999) and Mukherjee et al. (2003a) derive constraints on cosmological parameters from these data. Coble et al. (2003) also describe the procedure used to create maps of the sky with PyV and Python III data; these maps were compared to infer consistency and indirectly deduce the lack of significant foreground contamination in these data.

The PyV data were acquired at a frequency of ∼40 GHz. Two regions of sky covering 598 deg^2 in the southern hemisphere were observed (the "main PyV" region and a smaller region, the fields labeled "sa," "sb," and "sc" in Coble et al. 2003, that encompasses the region scanned earlier by the University of California at Santa Barbara South Pole 1994 experiment, hereafter the "SP94 overlap" region). There were 690 fields scanned in all (345 effective fields were scanned with two detector feeds separated by 2°.8 in azimuth on the sky) with an asymmetric Gaussian beam of FWHM 0°.94 × 1°.02. Once the telescope was positioned on each field, the chopper smoothly scanned in azimuth with a throw of 17°, 128 samples were recorded in each chopper cycle, and 164 chopper cycles of data were taken of a given field. The densely sampled data were then modulated in software using the first eight cosine harmonics of the chopper cycle (hereafter modulations, or in the tables, mods, 1–8). The modulations approach used has the advantage of filtering out some of the contaminants in the time stream and also provides a rapid means of compressing a large amount of data into a more manageable size. All the modulations, other than the first, were apodized by a Hann window to reduce ringing in multipole space and downweight data taken during chopper turnaround. The resulting data are sensitive to angular scales corresponding to multipole moments ranging from $l \sim 40$ to ∼260. More details about the particular observing strategy employed and results found, such as the angular power spectrum of the data, can be found in Coble et al. (2003); see Souradeep & Ratra (2001) for details about the window functions.

For this foreground analysis, we follow the general method outlined, for example, in Hamilton & Ganga (2001) and Mukherjee et al. (2002), doing a multimodulation analysis here rather than the multi- (frequency) channel analysis discussed in these papers. In doing so we extend the preliminary estimate presented in Coble et al. (1999). Here we use the technique of Souradeep & Ratra (2001) to account for correlations between modulations, in data that are sensitive

[1] Department of Physics, 116 Cardwell Hall, Kansas State University, Manhattan, KS 66506.
[2] Current address: Department of Physics and Astronomy, 440 West Brooks Street, University of Oklahoma, Norman, OK 73019.
[3] Enrico Fermi Institute, 5640 South Ellis Avenue, University of Chicago, Chicago, IL 60637.
[4] Adler Planetarium and Astronomy Museum, 1300 South Lake Shore Drive, Chicago, IL 60605.
[5] Jet Propulsion Laboratory, 4800 Oak Grove Drive, California Institute of Technology, MS 169-506, Pasadena, CA 91109.
[6] Infrared Processing and Analysis Center, California Institute of Technology, MS 100-22, Pasadena, CA 91125.
[7] Permanent address: IUCAA, Post Bag 4, Ganeshkhind, Pune 411007, India.

to a substantial range of angular scales, as well as compare with what has been found from the SP94 experiment (Gundersen et al. 1995; Ganga et al. 1997) data about foreground contamination in part of the PyV region (Hamilton & Ganga 2001; Mukherjee et al. 2002).

CMB data have previously been correlated with foreground templates (Differential Microwave Radiometer [DMR]: Kogut et al. 1996a, 1996b; 19 GHz survey: de Oliveira-Costa et al. 1998; Saskatoon experiment: de Oliveira-Costa et al. 1997; Owens Valley Radio Observatory [OVRO]: Leitch et al. 1997, Mukherjee et al. 2002; SP94: Hamilton & Ganga 2001, Mukherjee et al. 2002; Tenerife experiment: de Oliveira-Costa et al. 1999, 2002, Mukherjee et al. 2001; QMAP: de Oliveira-Costa et al. 2000; MAX: Lim et al. 1996, Ganga et al. 1998; and BOOMERANG: Masi et al. 2001).[8] Correlations between CMB data and infrared emission seem to be roughly consistent with free-free emission, spectrally, over a wide range of frequencies (10–90 GHz) and angular scales ($7°$ to $7'$), with some evidence for a contribution from spinning dust emission with a peak around 15–20 GHz. In general, however, the contamination from foregrounds has not been found to be large in any experiment, but on the detail level residual foregrounds can cause problems with parameter estimation and non-Gaussianity tests for high-precision CMB data.[9]

To model diffuse Galactic emission, we use the 100 μm IRAS+DIRBE map (Schlegel, Finkbeiner, & Davis 1998) as a tracer of thermal emission from interstellar dust and the 12 μm map (D. Finkbeiner 2000, private communication) as a tracer of emission from ultrasmall dust grains. Emission from small dust grains is still under study (Finkbeiner et al. 2002). Such grains may contribute significantly at microwave frequencies according to a model by Draine & Lazarian (1998a, 1998b), and this has been reviewed from the CMB data point of view by Kogut (1999) and Draine & Lazarian (1999). The Haslam 408 MHz map (Haslam et al. 1981) of synchrotron emission was not used, since it does not have enough resolution for all the modulations of the PyV experiment to be simulated on it. At the same time, synchrotron emission is not likely to contribute significantly at 40 GHz. We have tried to use Southern Hα Sky Survey Atlas data (Gaustad et al. 2001) as tracers of free-free emission but found that the template has insufficient resolution for our purpose.

We also use two point-source templates created from the Parkes-MIT-NRAO (PMN) survey (Wright et al. 1994). The one called PMN has been converted to δT_{CMB} (equivalent temperature fluctuations in the CMB at 40 GHz) using the spectral indexes given in the survey, while the one called PMN0 is converted to a flux at 40 GHz assuming a flat spectrum extrapolated from the flux measurement at 4.85 GHz. The assumption of a flat spectrum is conservative in that it is likely to overestimate the flux at 40 GHz. Neither case is correct, since spectral indexes have not been measured for all of the sources, in which case a flat spectrum is assumed. The two cases cover a reasonable range of possibilities. These templates were also used in the preliminary foreground analysis of Coble et al. (1999).

Each of the Galactic emission maps have been converted into a template for cross-correlation with the PyV data by simulating the PyV observing strategy on it, taking account of the asymmetric beam. Since a chopper synchronous offset and a ground shield offset were removed from the data, we account for this by adding the chopper synchronous offset and ground shield constraint matrices to the noise matrix and marginalizing over them in the analysis. The CMB theory covariance matrix is modeled using a spatially flat cosmological-constant–dominated cold dark matter model with nonrelativistic matter density parameter $\Omega_0 = 0.3$, scaled baryonic matter density parameter $\Omega_B h^2 = 0.021$ (here h is the present value of the Hubble parameter in units of 100 km s^{-1} Mpc^{-1}), and age $t_0 = 14$ Gyr (Ratra et al. 1999a), with the CMB anisotropy normalized to a quadrupole moment amplitude $Q_{rms\text{-}PS} = 20 \mu$K.

2. CORRELATIONS

2.1. Method

We follow the general method outlined, for example, in Hamilton & Ganga (2001) and Mukherjee et al. (2002), doing a multimodulation analysis here rather than the multi- (frequency) channel analysis discussed in these papers. The method assumes that the data are a linear combination of CMB anisotropies and foreground components:

$$y = aX + x_{CMB} + n . \quad (1)$$

Here y is an $n \times N$ element vector containing the data, n is the corresponding noise vector, x_{CMB} is the CMB signal, and X is an $(n \times N) \times n$ element matrix containing the simulated foreground template, N being the number of data points per modulation and n_{mod} being the number of modulations. In a given column, X contains mostly zeros except for the rows corresponding to that modulation, where it contains the simulated template signal. The vector a contains n_{mod} elements that represent the amplitude of the correlated foreground signal. If the noise and CMB anisotropies are uncorrelated Gaussian distributed variables with zero mean, minimizing χ^2 leads to a best-fit estimate of

$$\hat{a} = [X^T C^{-1} X]^{-1} X^T C^{-1} y , \quad (2)$$

where C is the $(n \times N) \times (n \times N)$ element total covariance matrix (sum of the theory covariance matrix that models the CMB signal, the noise covariance matrix, and any constraint matrices). The vector $\hat{a}$ then contains the best estimate for the correlation slopes for the corresponding template for all modulations, given all information about

---

[8] The Degree Angular Scale Interferometer (Halverson et al. 2002) and the Very Small Array (VSA; Taylor et al. 2002) are interferometric experiments that observe at frequencies of 26–36 GHz and are sensitive to multipoles of ~100–900. Point sources are the dominant source of contamination, and the effect of contamination from diffuse Galactic foregrounds on the CMB power spectrum is inferred to be small for both data sets. A full cross-correlation analysis of VSA data is underway (C. Dickinson et al. 2003, in preparation).

[9] The CMB anisotropy is often thought to have been generated by quantum mechanical fluctuations in a weakly coupled scalar field during an early epoch of inflation and thus would be a realization of a spatially stationary Gaussian random process (see, e.g., Ratra 1985; Fischler, Ratra, & Susskind 1985). Measurements lend fairly strong support to this Gaussianity assumption (see, e.g., Park et al. 2001; Shandarin et al. 2002; Santos et al. 2002; Polenta et al. 2002). See Park, Park, & Ratra (2002) for the effects of foreground contamination on Gaussianity tests based on anticipated MAP data.

intermodulation correlations. The matrix

$$\Sigma = \langle \hat{a}^2 \rangle - \langle \hat{a} \rangle^2 = \left[X^T C^{-1} X \right]^{-1} \qquad (3)$$

is its covariance matrix. The rms amplitude of temperature fluctuations in the data that results from the correlation is $\Delta T = (\hat{a} \pm \delta\hat{a})\sigma_{\mathrm{fore}}$, where σ_{fore} contains the rms deviations of the corresponding foreground template in the different modulations.

The method assumes that our foreground emission maps are good enough to model the foregrounds in the data accurately in all the different modulations, at a frequency different from that of the original foreground emission map, and that equation (1) explains all the structure in all modulations of the data. If we further assume that the ratio of the signal in the data to that in the foreground template is the same for all the modulations, then a net correlation slope can be found using

$$\bar{a} = \frac{\mathrm{Total}(\Sigma^{-1}a)}{\mathrm{Total}(\Sigma^{-1})} \ . \qquad (4)$$

Here Total denotes the sum of all elements of a matrix or vector. This is thus a weighted average taking account of correlations between the a-values of the different modulations. We can choose not to treat all modulations the same (see discussion in § 2.3). The error bar on $\bar{a}$ is $\{[\mathrm{Total}(\Sigma^{-1})]^{-1}\}^{1/2}$.

2.2. Results

The correlation slopes obtained from a complete intermodulation analysis using all the PyV data points, for each foreground emission template individually, are given in Table 1. We do not find any significant correlation. The net correlation slopes (i.e., the weighted mean of the correlation slopes given in the table, taking cross-modulation correlations into account) are not significant, with 2 σ upper limits of 34 μK (MJy sr^{-1})$^{-1}$, 110 μK (MJy sr^{-1})$^{-1}$, 156 μK μK^{-1}, and 897 μK (MJy sr^{-1})$^{-1}$ for the 100 μm, 12 μm, PMN, and PMN0 templates, respectively. These limits on the 100 μm and PMN0 correlation slopes compare well with those of Table 2 of Coble et al. (1999). (There are some errors in the PMN correlation slopes of their Table 2 and the rms values in Table 3 of Coble et al. 1999.) The upper limits obtained from using all modulations of the data together are given in Table 3.

The results of repeating this analysis for just the SP94 overlap region are also given in Table 1.[10] The uncertainties in the estimated correlation slopes are higher here, with the number of data points down by a factor of almost 8 (the time spent observing this region was less than one-eighth of the total observing time), but the level of associated temperature fluctuations is relatively higher, at least for the 100 μm template. As seen from Tables 2 and 3, the rms of the data and the 100 μm template are higher in this patch of sky. Again, no significant correlations are found. The weighted correlation coefficient between foreground emission templates is given by $\Sigma_{ij}^{-1}(\Sigma_{ii}^{-1}\Sigma_{jj}^{-1})^{-0.5}$ (de Oliveira-Costa et al.

1999). The 100 and 12 μm templates and the PMN and PMN0 templates are found to have significant weighted correlation coefficients in this region of sky, with the correlation reducing somewhat, from 0.7 to 0.5, with increasing modulation for the two dust templates, while it remains steady at about 0.85 for the two point-source templates. (These templates are much less like each other when all the PyV fields are considered.) However, when all modulations of the data are analyzed together, joint template fits do not detect any correlations. The net correlation slopes obtained from a complete intermodulation analysis of the SP94 overlap region are not significant, with 2 σ upper limits of 69 μK (MJy sr^{-1})$^{-1}$, 1027 μK (MJy sr^{-1})$^{-1}$, 603 μK μK^{-1}, and 2198 μK (MJy sr^{-1})$^{-1}$, for the 100 μm, 12 μm, PMN, and PMN0 templates, respectively. The upper limits obtained from using all modulations of the data together are given in Table 3.

2.3. Low-l Modulations

As seen from Table 2, the signal in the foreground templates falls more steeply with increasing modulation number than do the data, so the case here, of fitting for several modulations simultaneously, is somewhat different from the case of fitting multifrequency data: if a certain foreground is present in the data, picking it out in the higher modulations will be more difficult. However, the cumulative effect of the other modulations is significant on the estimated correlation slope for any modulation; Figure 2 of Coble et al. (1999) shows how much the CMB signals in different modulations overlap. Hence, simultaneously fitting for the correlation slopes in all the modulations of the data may not be the most appropriate thing to do. It is also important to note that the foregrounds may not have been accurately modeled in the higher modulations because of insufficient resolution (given the dense sampling in the data). There may also be different kinds of unmodeled or incorrectly modeled foregrounds/ errors in different modulations. Hence, it is useful to also look at the results from analyzing, for instance, the first three modulations together, because across these modulations, the data and the foreground signal seem to be roughly similar as regards rms values, or each modulation individually, at the cost of increased uncertainty in the estimates.

If we look at only the first modulation in the SP94 overlap region, we find a 1.8 σ correlation slope of 80 ± 45 μK (MJy sr^{-1})$^{-1}$ (36 ± 21 μK) for the 100 μm template (Table 4). For the 12 μm template, the correlation found is just less than 1 σ, but here the two dust templates have a weighted correlation coefficient of 0.65, and performing a joint correlation of the data with these two templates results in a 1.9 σ correlation slope of 115 ± 60 μK (MJy sr^{-1})$^{-1}$ (52 ± 27 μK) for the 100 μm template at the cost of a 1 σ negative correlation with the 12 μm template. This may be the signal found in the foreground analysis of the SP94 data (Hamilton & Ganga 2001; Mukherjee et al. 2002; for earlier qualitative indications, see Ganga et al. 1997; Ratra et al. 1999b). While there a detection was aided by the presence of seven frequency channels, here the error bars for the individual modulation correlations are large. This could be just a chance correlation on the other hand, and the probability of that is reflected in the significance of the result. It might also be relevant to note here that the SP94 data were only one-dimensional, while here the PyV sa, sb, and sc data are essentially two-dimensional.

---

[10] An outlier that affects six data points per feed per modulation is seen in the 12 μm template; hence, these data points are ignored whenever this region is being analyzed. Outliers are more difficult to pick out over larger regions of sky, but they also affect the result less, so nothing is removed when analyzing the full data set.

TABLE 1
RESULTS OF CORRELATING THE PγV DATA WITH INDIVIDUAL FOREGROUND EMISSION TEMPLATES[a]

Template	Mod 1	Mod 2	Mod 3	Mod 4	Mod 5	Mod 6	Mod 7	Mod 8
Whole PγV Region								
100 μm:								
Correlation slope...........	1 ± 20	−4 ± 20	−20 ± 20	−6 ± 23	5 ± 30	8 ± 52	−34 ± 110	−172 ± 245
Temperature fluctuation.........	0 ± 4	−1 ± 3	−2 ± 2	0 ± 2	0 ± 1	0 ± 1	0 ± 1	−1 ± 1
12 μm:								
Correlation slope...........	−82 ± 131	−75 ± 123	−79 ± 120	−133 ± 126	−257 ± 140	−372 ± 182	−228 ± 259	−476 ± 516
Temperature fluctuation.........	−2 ± 3	−2 ± 3	−1 ± 2	−2 ± 2	−3 ± 1	−3 ± 1	−1 ± 1	−1 ± 1
PMN:								
Correlation slope...........	137 ± 123	66 ± 108	−14 ± 103	−68 ± 100	−158 ± 105	−173 ± 126	−137 ± 177	8 ± 252
Temperature fluctuation.........	3 ± 3	2 ± 3	0 ± 2	−1 ± 2	−2 ± 1	−2 ± 1	−1 ± 1	0 ± 1
PMN0:								
Correlation slope...........	684 ± 502	546 ± 408	237 ± 382	15 ± 369	−111 ± 385	−116 ± 452	−44 ± 625	972 ± 986
Temperature fluctuation.........	3 ± 2	3 ± 2	1 ± 1	0 ± 1	0 ± 1	0 ± 1	0 ± 1	1 ± 1
SP94 Overlap Region								
100 μm:								
Correlation slope...........	19 ± 30	18 ± 30	5 ± 31	12 ± 35	30 ± 50	92 ± 94	−104 ± 266	792 ± 1051
Temperature fluctuation.........	8 ± 14	6 ± 11	1 ± 7	2 ± 6	3 ± 5	4 ± 4	−2 ± 4	4 ± 5
12 μm:								
Correlation slope...........	116 ± 570	235 ± 559	−288 ± 561	−248 ± 647	−348 ± 868	−626 ± 1672	−2476 ± 3871	7207 ± 11467
Temperature fluctuation.........	2 ± 12	4 ± 10	−4 ± 7	−2 ± 6	−2 ± 6	−2 ± 5	−3 ± 5	4 ± 6
PMN:								
Correlation slope...........	205 ± 327	98 ± 291	70 ± 266	5 ± 276	78 ± 320	−123 ± 436	319 ± 801	862 ± 1717
Temperature fluctuation.........	5 ± 8	3 ± 8	1 ± 6	0 ± 4	1 ± 4	−1 ± 3	1 ± 4	3 ± 5
PMN0:								
Correlation slope...........	1871 ± 2030	947 ± 1722	636 ± 1607	267 ± 1645	409 ± 1958	−1496 ± 2851	3495 ± 5538	9599 ± 11042
Temperature fluctuation.........	8 ± 8	5 ± 8	2 ± 6	1 ± 5	1 ± 4	−2 ± 4	3 ± 4	5 ± 6

[a] For each template, the correlation slopes (in units of μK [MJy sr^{-1}]$^{-1}$ for the dust and the PMN0 templates and in units of μK μK^{-1} for the PMN template) are given in the first row, and the corresponding temperature fluctuations (in μK) are given in the second row. In the top half we use all the data points, and in the bottom half we use only the fields in the SP94 overlap region. Cross-modulation correlations are accounted for, and the eight modulations represent decreasing angular scales covering $l \sim 40$ to ~ 260.

TABLE 2
rms Values of the Signal in the PyV Data and the Templates[a]

Modulation	Data (μK)	100 μm (MJy sr^{-1})	12 μm (MJy sr^{-1})	PMN (μK)	PMN0 (MJy sr^{-1})
Whole PyV Region					
1.............................	92.0	0.222	0.022	0.022	0.004
2.............................	95.1	0.170	0.022	0.027	0.006
3.............................	79.4	0.100	0.019	0.022	0.005
4.............................	77.0	0.078	0.015	0.017	0.004
5.............................	78.6	0.047	0.010	0.013	0.003
6.............................	77.4	0.023	0.007	0.010	0.002
7.............................	69.8	0.011	0.006	0.007	0.002
8.............................	65.0	0.006	0.003	0.005	0.001
SP94 Overlap Region					
1.............................	123.0	0.455	0.022	0.025	0.004
2.............................	129.9	0.356	0.018	0.028	0.005
3.............................	104.9	0.221	0.013	0.022	0.004
4.............................	111.1	0.180	0.010	0.016	0.003
5.............................	113.6	0.103	0.007	0.012	0.002
6.............................	111.5	0.042	0.003	0.008	0.001
7.............................	95.7	0.015	0.001	0.004	0.001
8.............................	89.33	0.005	0.001	0.003	0.0005

[a] The top half is for the whole PyV region with 690 fields per modulation. The bottom half is for the SP94 overlap region with 90 fields per modulation.

TABLE 3
Correlation Slopes

Fields	Modulations	100 μm (μK [MJy sr^{-1}]$^{-1}$)	12 μm (μK [MJy sr^{-1}]$^{-1}$)	PMN (μK μK^{-1})	PMN0 (μK [MJy sr^{-1}]$^{-1}$)
All..............................	All	-4 ± 19	-120 ± 115	-30 ± 93	209 ± 344
SP94 overlap	All	13 ± 28	-21 ± 524	85 ± 259	904 ± 1551

TABLE 4
Correlation Slopes for Low-l Modulations[a]

Modulations	100 μm (μK [MJy sr^{-1}]$^{-1}$)	12 μm (μK [MJy sr^{-1}]$^{-1}$)	PMN (μK μK^{-1})	PMN0 (μK [MJy sr^{-1}]$^{-1}$)
Whole PyV Region				
First three mods	7 ± 22	-155 ± 141	-59 ± 131	203 ± 553
First two mods	16 ± 24	-70 ± 162	-77 ± 154	416 ± 658
First mod	$29 \pm 29^*$	97 ± 223	-161 ± 213	213 ± 903
Second mod	$29 \pm 33^*$	-27 ± 202	-53 ± 190	271 ± 779
SP94 Overlap Region				
First three mods	$33 \pm 32^*$	388 ± 590	-129 ± 332	-283 ± 1924
First two mods	$50 \pm 36^*$	522 ± 674	-6 ± 387	736 ± 2215
First mod	$80 \pm 45^*$	406 ± 875	190 ± 563	2131 ± 3401
Second mod	$49 \pm 47^*$	854 ± 889	65 ± 473	-158 ± 2805

[a] Values marked with an asterisk indicate a 1 σ detection.

If we look at only the second modulation by itself, the correlation slopes are as shown in Table 4, and even though the correlation coefficient between the 12 and 100 μm templates is 0.70, nothing is gained by a joint fit this time.

In the first two modulations together, some correlation with the 100 μm template is detected, consistent with the above estimates. When the first three modulations are correlated simultaneously, a 1.6 σ correlation slope of 58 ± 36 μK (MJy sr^{-1})$^{-1}$ (25 ± 16 μK) is found with the 100 μm template in the first modulation and a 1 σ 710 ± 695 μK (MJy sr^{-1})$^{-1}$ (14 ± 14 μK) correlation is found with the 12 μm template in the second modulation. The correlation coefficient between the templates is high, and correlations of similar significance are found in the same modulations when the two templates are analyzed jointly.

Regarding the point-source templates, nothing significant shows up in an individual template analysis (Table 4). When analyzing the first two modulations together, the two point-source templates have a correlation coefficient of 0.8, and a correlation slope of 6555 ± 4994 μK (MJy sr^{-1})$^{-1}$ (28 ± 21 μK) at 1.3 σ is found with the PMN0 template in modulation 1 at the cost of a 1 σ negative correlation with the PMN template in the same modulation. When analyzing the first three modulations together, the point-source templates have a high correlation coefficient, and a 1.2 σ correlation of 5625 ± 4498 μK (MJy sr^{-1})$^{-1}$ (24 ± 19 μK) is found with the PMN0 template in modulation 1 at the cost of a -1 σ correlation with the PMN template in the same modulation.

When all the PyV fields are taken together (690 in each modulation), a 1 σ correlation with the 100 μm template shows up in the first modulation (when the first modulation is analyzed by itself, jointly with the second, or jointly with the second and third), and a 1 σ correlation with the PMN0 template shows up in the first modulation when it is analyzed together with the second modulation and jointly with the PMN template. The uncertainty in the correlation slopes with the point-source templates is lowest in the third and fourth modulations, but nothing significant shows up when these modulations are analyzed separately. Hence, consistent correlations (in the low-l modulations and at low significance) are seen even when both of the PyV regions are analyzed together.

2.4. Summary

When all the modulations of the data are analyzed together, no significant correlations are found in the whole PyV data set or in the SP94 overlap region. These results are summarized in Table 3 and plotted in Figure 1.

We have discussed the motivations for looking at individual modulations separately, and we find some indication of foregrounds in the low-l modulations. Correlation slopes for some of these low-l modulations are summarized in Table 4. We see that greater than 1 σ correlations show up in the SP94 overlap region with the 100 μm template in particular, but also with the 12 μm template and the PMN0 template in some modulations in a joint modulation analysis of a few modulations. In addition, consistent correlations are seen when all the PyV data fields are analyzed together.

We note that according to the foreground model discussed, for example, in Mukherjee et al. (2002), if the 100 μm correlations are from both free-free emission and spinning dust emission, then by 40 GHz the contribution from spinning dust emission (as traced by the 12 μm template)

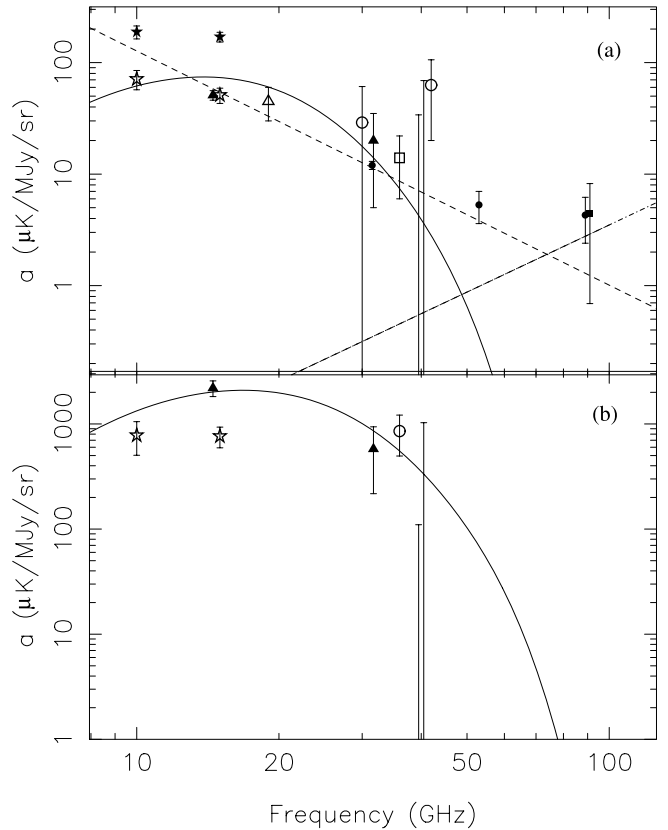Fig. 1.—(*a*) Correlation slopes between CMB anisotropy data and the dust 100 μm template. The 2 σ upper limits obtained for PyV from analyzing all the fields and from analyzing the SP94 overlap region only are both shown at ~40 GHz. (*b*) Correlations with the 12 μm template. Results are also shown for other experiments: Tenerife (*open stars*: de Oliveira-Costa et al. 2002; *filled stars*: Mukherjee et al. 2001), OVRO (*filled triangles*), 19 GHz (*open triangles*), SP94 (*open circles*), Saskatoon (*open square*), BOOMERANG (*filled rectangle*), and DMR (*filled circles*). The solid curves are representative of a spinning dust spectrum, and the dashed and the dot-dashed lines represent free-free and vibrational dust emission spectra, respectively.

may have again dropped below that from free-free emission (the frequency at which spinning dust emission peaks depends on the details of the spinning dust emission model, and this can also vary from region to region), so that we would expect 100 μm correlations to be more significant than 12 μm correlations at this frequency (see Fig. 1*a*). However, given the error bars (the numbers in Table 4), we do not expect to see significant correlations in the PyV data (see Fig. 1).

3. CONCLUSION

Using the method of cross-correlating CMB anisotropy data with foreground contaminant emission templates, we find little evidence for foreground contamination in the whole PyV region when analyzing all modulations of the data together. There is, however, indication of foreground contamination in the low-l modulations of the PyV fields that cover the region scanned earlier by the SP94 experiment, consistent with results from the SP94 data. This is a valuable test, indicating consistency between results found using data from two different experiments. Given the

uncertainties, our findings are not inconsistent with the two-component dust-correlated (free-free and spinning dust) foreground emission model that other data sets tentatively seem to point to (Mukherjee et al. 2002).

REFERENCES

Benoît, A., et al. 2003, A&A, 399, L25
Coble, K., Dodelson, S., Dragovan, M., Ganga, K., Knox, L., Kovac, J., Ratra, B., & Souradeep, T. 2003, ApJ, 584, 585
Coble, K., et al. 1999, ApJ, 519, L5
de Oliveira-Costa, A., Kogut, A., Devlin, M. J., Netterfield, C. B., Page, L. A., & Wollack, E. J. 1997, ApJ, 482, L17
de Oliveira-Costa, A., Tegmark, M., Gutierrez, C. M., Jones, A. W., Davies, R. D., Lasenby, A. N., Rebolo, R., & Watson, R. A. 1999, ApJ, 527, L9
de Oliveira-Costa, A., Tegmark, M., Page, L. A., & Boughn, S. P. 1998, ApJ, 509, L9
de Oliveira-Costa, A., et al. 2000, ApJ, 542, L5
———. 2002, ApJ, 567, 363
Dragovan, M., Ruhl, J. E., Novak, G., Platt, S. R., Crone, B., Pernic, R., & Peterson, J. B. 1994, ApJ, 427, L67
Draine, B. T., & Lazarian, A. 1998a, ApJ, 494, L19
———. 1998b, ApJ, 508, 157
———. 1999, in ASP Conf. Ser. 181, Microwave Foregrounds, ed. A. de Oliveira-Costa & M. Tegmark (San Francisco: ASP), 133
Finkbeiner, D. P., Schlegel, D. J., Frank, C., & Heiles, C. 2002, ApJ, 566, 898
Fischler, W., Ratra, B., & Susskind, L. 1985, Nucl. Phys. B, 259, 730
Ganga, K., Ratra, B., Gundersen, J. O., & Sugiyama, N. 1997, ApJ, 484, 7
Ganga, K., Ratra, B., Lim, M. A., Sugiyama, N., & Tanaka, S. T. 1998, ApJS, 114, 165
Gaustad, J. E., McCullough, P. R., Rosing, W., & Van Buren, D. 2001, PASP, 113, 1326
Gundersen, J. O., et al. 1995, ApJ, 443, L57
Halverson, N. W., et al. 2002, ApJ, 568, 38
Hamilton, J.-Ch., & Ganga K. M. 2001, A&A, 368, 760
Haslam, C. G. T., Klein, U., Salter, C. J., Stoffel, H., Wilson, W. E., Cleary, M. N., Cooke, D. J., & Thomasson, P. 1981, A&A, 100, 209
Kogut, A. 1999, in ASP Conf. Ser. 181, Microwave Foregrounds, ed. A. de Oliveira-Costa & M. Tegmark (San Francisco: ASP), 91
Kogut, A., Banday, A. J., Bennett, C. L., Górski, K. M., Hinshaw, G., & Reach, W. T. 1996a, ApJ, 460, 1
Kogut, A., Banday, A. J., Bennett, C. L., Górski, K. M., Hinshaw, G., Smoot, G. F., & Wright, E. L. 1996b, ApJ, 464, L5
Kuo, C. L., et al. 2002, ApJ, submitted (astro-ph/0212289)
Leitch, E. M., Readhead, A. C. S., Pearson, T. J., & Myers, S. T. 1997, ApJ, 486, L23

Lim, M. A., et al. 1996, ApJ, 469, L69
Masi, S., et al. 2001, ApJ, 553, L93
Mukherjee, P., Dennison, B., Ratra, B., Simonetti, J. H., Ganga, K., & Hamilton, J.-Ch. 2002, ApJ, 579, 83
Mukherjee, P., Ganga, K., Ratra, B., Rocha, G., Souradeep, T., Sugiyama, N., & Górski, K. M. 2003a, Intl. J. Mod. Phys., in press
Mukherjee, P., Jones, A. W., Kneissl, R., & Lasenby, A. N. 2001, MNRAS, 320, 224
Mukherjee, P., Souradeep, T., Ratra, B., Sugiyama, N., & Górski, K. M. 2003b, Mod. Phys. Lett. A, 18, 1145
Page, L. 2002, in New Trends in Theoretical and Observational Cosmology: Proc. 5th RESCEU Intl. Symp., ed. K. Sato & T. Shiromizu (Tokyo: Universal Academy Press)
Park, C.-G., Park, C., & Ratra, B. 2002, ApJ, 568, 9
Park, C.-G., Park, C., Ratra, B., & Tegmark, M. 2001, ApJ, 556, 582
Peebles, P. J. E., & Ratra, B. 2003, Rev. Mod. Phys., 75, 559
Platt, S. R., Kovac, J., Dragovan, M., Peterson, J. B., & Ruhl, J. E. 1997, ApJ, 475, L1
Podariu, S., Souradeep, T., Gott, J. R., Ratra, B., & Vogeley, M. S. 2001, ApJ, 559, 9
Polenta, G., et al. 2002, ApJ, 572, L27
Ratra, B. 1985, Phys. Rev. D, 31, 1931
Ratra, B., Ganga, K., Stompor, R., Sugiyama, N., de Bernardis, P., & Górski, K. M. 1999a, ApJ, 510, 11
Ratra, B., Stompor, R., Ganga, K., Rocha, G., Sugiyama, N., & Górski, K. M. 1999b, ApJ, 517, 549
Rocha, G., Stompor, R., Ganga, K., Ratra, B., Platt, S. R., Sugiyama, N., & Górski, K. M. 1999, ApJ, 525, 1
Ruhl, J. E., Dragovan, M., Platt, S. R., Kovac, J., & Novak, G. 1995, ApJ, 453, L1
Ruhl, J. E., et al. 2002, preprint (astro-ph/0212229)
Santos, M. G., et al. 2002, Phys. Rev. Lett., 88, 241302
Schlegel, D. J., Finkbeiner, D. P., & Davis, M. 1998, ApJ, 500, 525
Shandarin, S. F., Feldman, H. A., Xu, Y., & Tegmark, M. 2002, ApJS, 141, 1
Slosar, A., et al. 2003, MNRAS, 341, L29
Souradeep, T., & Ratra, B. 2001, ApJ, 560, 28
Taylor, A. C., et al. 2002, MNRAS, in press
Wright, A. E., Griffith, M. R., Burke, B. F., & Ekers, R. D. 1994, ApJS, 91, 111